Oceanic forcing of the wintertime North Atlantic Oscillation and European climate

M. J. Rodwell*, D. P. Rowell* & C. K. Folland*

* Hadley Centre for Climate Prediction and Research, UK Meteorological Office, London Road, Bracknell RG12 2SY, UK

The weather over the North Atlantic Ocean, particularly in winter, is often characterized by strong eastward air-flow between the 'Icelandic low' and the 'Azores high', and by a 'stormtrack' of weather systems which move towards western Europe. The North Atlantic Oscillation—an index of which can be defined as the difference in atmospheric pressure at sea level between the Azores and Iceland—is an important mode of variability in the global atmosphere[1,2] and is intimately related to the position and strength of the North Atlantic stormtrack owing to dynamic processes internal to the atmosphere[3,4]. Here we use a general circulation model of the atmosphere to investigate the ocean's role in forcing North Atlantic and European climate. Our simulations indicate that much of the multiannual to multidecadal variability of the winter North Atlantic Oscillation over the past half century may be reconstructed from a knowledge of North Atlantic sea surface temperature. We argue that sea surface temperature characteristics are 'communicated' to the atmosphere through evaporation, precipitation and atmospheric-heating processes, leading to changes in temperature, precipitation and storminess over Europe. As it has recently been proposed that there may be significant multiannual predictability of North Atlantic sur-face temperature patterns[5], our results are encouraging for the prediction of European winter climate up to several years in advance.

It has been long recognized that fluctuations in sea surface temperature (SST) and the strength of the North Atlantic Oscillation (NAO) in the North Atlantic are related[6]. For example, stronger eastward flow generally increases evaporation, thereby cooling SST[6–9]. On the other hand, SST anomalies, including those in middle latitudes, have been thought to be partly responsible for changes in atmospheric circulation over the North Atlantic and Europe in winter or spring[10–13]. A mechanism has been proposed[14,15] that involves a positive feedback between the ocean and atmosphere. Other authors, however, find little evidence of positive feedbacks[16,17].

The global atmospheric model used in this study is the HadAM2b version of the UK Meteorological Office's Unified Model[18]. It has a horizontal grid resolution of $2.5° \times 3.75°$ in latitude and longitude with 19 hybrid σ, p levels in the vertical and a timestep of 30 min. The model incorporates prognostic cloud water and ice, has a mass-flux convection scheme with stability closure and uses mean orography. It was forced with observed SSTs and sea-ice extents taken from the GISST3.0 data set (N. Rayner, personal communication). An ensemble of six 128-year simulations were started from 1870, differing only in their initial atmospheric conditions. By taking averages of this ensemble, atmospheric 'noise' can be substantially reduced. Here, we discuss the period 1947–97 when oceanic data are thought to be most reliable. We focus on the December to February (DJF) season when, through strong heat fluxes at the surface and a deeper mixed layer in the ocean[19], the atmosphere is likely to be most strongly linked to deeper ocean temperatures, which vary on the longer timescales of interest here.

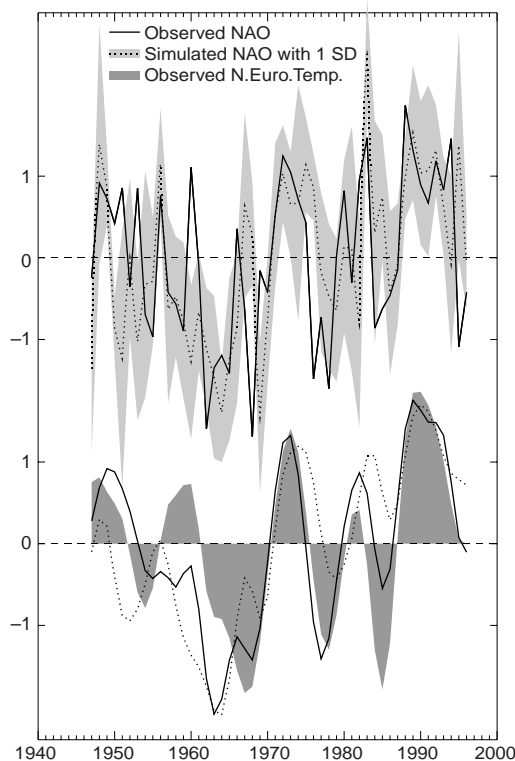Figure 1 shows that the model simulates well the observed decline

Figure 1 Time series of the North Atlantic Oscillation index. Observed (solid line) and modelled ensemble average (dotted line) winter NAO index, December to February 1947–97. The NAO index is calculated as the normalized difference in December to February mean sea-level pressure between the Azores (26° W 38° N) and Iceland (23° W 65° N). Observed data is taken from Ponta Delgada (Azores) and Stykkisholmur (Iceland). The shading in the upper graph shows ±1 standard deviation about the ensemble mean, calculated from the normalized six model simulations for each individual year. The lower graph shows the NAO index time series after they have been filtered to pass variations with periods greater than 6.5 years (using a 1-2-1 binomial filter three times). Shading in the lower graph is the normalized filtered time series of observed North European surface temperatures (averaged over the box 5–50° E, 50–70° N). The year corresponds to December for each DJF season.

of the NAO to the 1960s, its subsequent rise to the early 1990s, and some of the recent smaller fall. Moreover, much of the multiannual variability and some interannual changes in the NAO have been captured. The correlation between the simulated and observed unfiltered curves is quite high at 0.41 (upper set of curves in Fig. 1) and significant at the 98% confidence level allowing for persistence. These curves show that, assuming SSTs are known, it may be possible to predict the correct sign of the winter NAO index in 2 out of 3 years. The sign of strong events (larger than one standard deviation) is correctly predicted 3 times out of 4. Each individual model simulation correlates more poorly with the observed NAO index than does the ensemble average, emphasizing the importance of making more than one model simulation. Internal variability in the real atmosphere still limits the accuracy of a forecast, although the observed NAO index does generally remain within ±1 standard deviation of the ensemble mean (indicated by the shading in the upper graph in Fig. 1). When internal variability is reduced by filtering the data to include only timescales longer than 6.5 years (lower curves in Fig. 1), the correlation rises to 0.74 which is significant at the 99.9% level, again allowing for persistence. Thus multiannual to multidecadal variations in the NAO are considerably better simulated than interannual timescales. This study uses an atmospheric model,
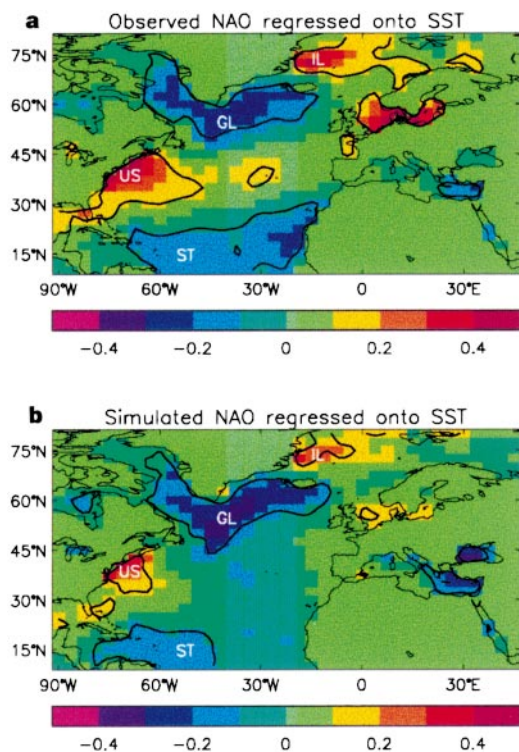
320 NATURE | VOL 398 | 25 MARCH 1999 | www.nature.com

Figure 2 NAO/SST regressions. **a**, Regression of the 50-year time series of observed unfiltered NAO index, as in Fig. 1, onto observed North Atlantic SST. Units are in K and correspond to an NAO index anomaly of 1 standard deviation. **b**, As **a** but for a regression of the unfiltered model ensemble averaged NAO index onto North Atlantic SST. The areas within the black contours exceed the 95% confidence level of non-zero correlation using a 2-tailed *t*-test. Regions 'ST', 'US', 'GL' and 'IL' are explained in the text.

without feedback onto the ocean, and hence the skill of our NAO simulations must result from the prescribed SSTs and sea ice. We note that any direct effect of changes in greenhouse gases or stratospheric ozone on the NAO is not included in this simulation, although indirect effects through the ocean surface would be included.

The NAO has a substantial effect on temperature and rainfall in Europe and the eastern United States[20–22]. The shading in the lower graph of Fig. 1 shows the filtered time series of observed North European surface temperatures. Their correlation with the observed NAO index is very high at 0.82 (the unfiltered correlation is 0.72), but the model does somewhat less well at capturing this link. The difference between the two 7-year winter periods December–February 1962–69 (low NAO index) and DJF 1987–94 (high NAO index) shows precipitation[23] increased by up to 30% in Britain and much of Scandinavia and decreased by 50% in southern Spain, Italy and Greece. Hence there are benefits to be gained, for instance for agriculture and the utilities[24], if skilful long-range forecasts of the NAO can be made.

Figure 2a shows the regression of the observed unfiltered NAO index onto SSTs for much of the North Atlantic region. The regression pattern, with negative centres in the subtropics (ST) and south of Greenland (GL) and positive centres off the east coast of the United States (US) and north of Iceland (IL), agrees well with previous results[5,6,13,15,25]. Outside the region shown, correlations are not field-significant (that is, the small percentage of points with appreciable correlations could have occurred by chance), with no locally statistically significant correlations in the tropical and northern Pacific Ocean or the South Atlantic Ocean. Neither is there any evidence of locally statistically significant correlation when the NAO index is regressed onto winter mean sea-level pressure (MSLP)

outside the North Atlantic region. These results suggest that El Niño and any pan-Atlantic SST mode[26] have little direct relationship to the NAO in this season[3] (unless in relatively rare circumstances). When the modelled ensemble mean NAO index is regressed onto the same SST data, a similar pattern emerges in the North Atlantic, Fig. 2b, suggesting that ocean to atmosphere forcing is important at this timescale and that the model correctly simulates the main mechanisms linking SSTs to the NAO, such as surface fluxes, atmospheric convection and any teleconnections within the North Atlantic region. Differences between Fig. 2a and b in the North Sea and Baltic and off the coast of northwest Africa may suggest that atmosphere to ocean forcing is dominant in these regions.

To confirm that North Atlantic SSTs do force the NAO, we use a North Atlantic SST pattern similar to Fig. 2a and b that is obtained from a canonical correlation analysis by Grötzner *et al.*[15] (Fig. 3a). It is appropriately scaled to force 20-year idealized simulations with the model. Maximum values of the SST forcing are about $\pm 1\,^{\circ}\mathrm{C}$. Figure 3b shows the difference in DJF MSLP between model simulations with positive (P) and negative (N) versions of this SST anomaly pattern. The atmospheric response is similar to the classical NAO pattern, although there are differences such as the centre of the 'Azores high' being about 5° too far north. A pressure difference of 6 hPa between the Azores and Iceland (Fig. 3b) is comparable with the standard deviation of the observed DJF NAO index. Surface temperature changes (not shown) over northern Europe, the eastern United States, Greenland and the Middle East are all consistent with the expected local thermal advection by the NAO wind field[20].

The same MSLP pattern is obtained when DJF MSLP from the ensemble of six simulations is regressed onto the time series of the SST anomaly pattern. The correlation between the SST pattern time series and the unfiltered observed and ensemble average NAO is 0.53 and 0.47, respectively (statistically significant at the 99.9% level). Multiple regression of the NAO onto time series of the SST anomaly centres GL, US and ST (Fig. 3a) suggests that GL and US are particularly important for forcing the NAO.

We now investigate the mechanism by which this SST signal might affect the atmosphere. Figure 3c shows the difference in evaporation from the ocean surface between model simulations P and N. The flux of latent heat by evaporation represents an important heat flux at the surface[7,8,17] and dominates other surface heat flux changes in P minus N. There is strong spatial coherence between Figs 3a and c, with increased evaporation in regions of positive SST anomalies and decreased evaporation in regions of negative SST anomalies. In middle latitudes, there is a secondary effect of a southward shift of the evaporation centre relative to the GL SST anomaly; this may be due to the increased sensitivity of evaporation to the warmer SSTs in the south of this region and also to feedbacks with the eastward wind. Figure 3d shows the difference in precipitation in terms of changes in the associated latent heat release and therefore in column-mean heating in the atmosphere. Comparing Fig. 3c and d, there is again strong spatial coherence with about 60% of the SST-forced changes in evaporation being 'rained-out' locally. Convective precipitation changes dominate this signal, although large-scale precipitation (slope convection) also makes an appreciable contribution in the middle latitudes.

As expected, changes in the atmospheric thermal structure, for instance in the thickness of the 200–925 hPa layer, are in quadrature with the changes in latent heating, with thermal anomalies centred immediately downstream of heating anomalies (Fig. 3d). This can be seen directly in the 200-hPa geopotential height anomalies, Fig. 3e, which are the dominant contributor to the thickness anomalies. Figure 3b and e indicate a near-equivalent barotropic vertical structure[2,4,28] with a deep 'low' near Iceland and the band of high pressure near 45° N extending throughout the troposphere. This height field strongly resembles the 'NAO' modes mentioned by other authors[4]. In the 'Azores high' region, although there are

undoubtedly feedbacks within the atmosphere, the indication is that local SSTs play a role in forcing the observed cooling, Fig. 3d (with a maximum at about 790 hPa), and hence are also important for the low-level anticyclonic circulation centred around 30° W, 45° N (Fig. 3b).

Hence we have demonstrated that North Atlantic SST anomalies can lead to local changes in surface evaporation, precipitation and atmospheric heating that tend to re-enforce the thermal and geopotential structure of the NAO[4]. This forcing of the NAO is distinct from the natural tendency of the NAO to damp diabatically[4]. We also find a northward shift and 13% intensification into northern Europe of the stormtrack, Fig. 3f. Such a shift has been associated with the pressure field of positive phases of the NAO[3],

although interactions between synoptic variations and the large-scale flow may complicate a simple interpretation[4].

We now briefly examine the implied changes in heat fluxes in the oceanic mixed layer between simulations P and N. Evaporation (Fig. 3c), which represents a cooling of the ocean, generally acts to damp the P minus N SST anomalies (Fig. 3a). The same result emerges from a regression analysis of the ensemble of simulations. Hence a positive feedback on SSTs involving evaporation, considered by previous authors[14,15], does not occur in this model. Ekman transport is another important term in the oceanic mixed-layer heat budget[7,17]. In the steady state, an anomalous eastward windstress in the Northern Hemisphere, for example, must be balanced by a Coriolis term, and hence by cold water advection from the north.
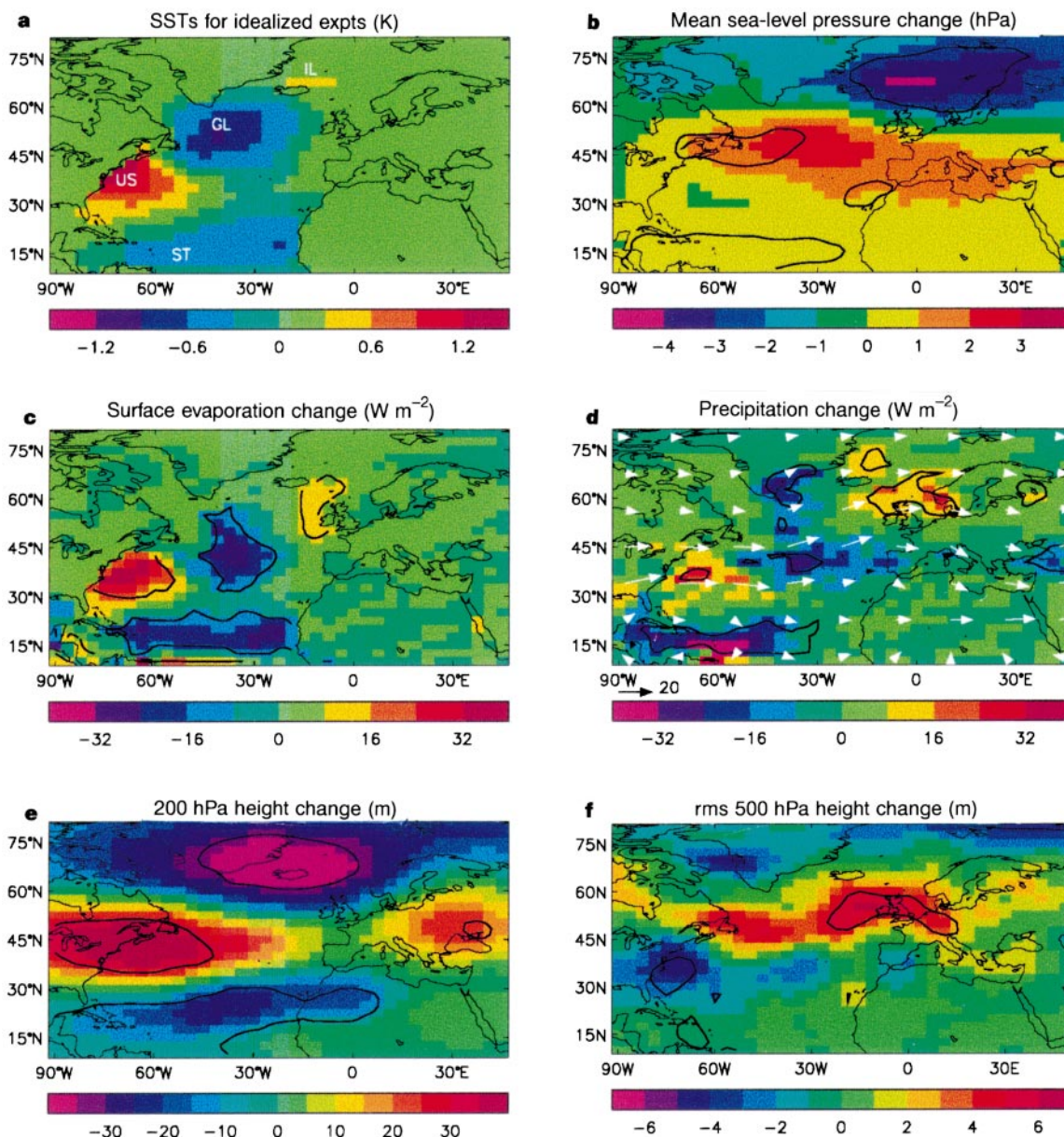

Figure 3 Model inputs and simulated responses. **a**, The pattern of SST anomalies used to force two 20-year model simulations, taken from a joint canonical correlation analysis on SSTs and MSLP[15]. The values shown correspond to the average of the monthly-varying SST anomalies used in the December to February season. For each month of the year, the scaling is calculated as two standard deviations of the time series obtained by projecting observed SSTs for that month onto the pattern. SST anomalies are added to (simulation P) or subtracted from (simulation N) a climatological SST field for 1961–90. **b**, December to February MSLP difference, simulation P minus simulation N. **c**, As **b**, but for surface evaporation in terms of latent heat flux (W m^{-2}). **d**, As **b** but for total precipitation in terms of condensational latent heat release (W m^{-2}). Superimposed are mean 500-hPa wind vectors calculated as the average of simulations P and N. The reference vector is 20 m s^{-1}. **e**, As **b** but for 200-hPa geopotential height. **f**, As **b** but for the 20-season mean of the r.m.s. of 2.5–6 day bandpass-filtered[27] daily 500-hPa height. In **b**–**f**, the areas within the black contours exceed the 95% confidence level of non-zero difference using a 2-tailed t-test.

We find that the Ekman transport provides a positive feedback to the P minus N SST anomaly over almost the entire North Atlantic and for most of the year. North of about 45° N, this term often provides a positive feedback that is stronger than any negative feedback from evaporation. Elsewhere, evaporation tends to be stronger.

We have provided evidence that simulations of the NAO in the HadAM2b model are influenced by a pattern of ocean surface temperatures which is similar to one of the most important naturally occurring patterns of North Atlantic SST variability[9]. Observational studies have shown that there may be significant predictability of mixed-layer oceanic temperatures in the North Atlantic at multiannual timescales[5] and these have been linked in observational studies to the NAO[29]. This suggests the possibility of multiannual, as well as seasonal, predictions of European winter climate features such as surface temperature, precipitation and storminess. Our use of an atmospheric model forced with imposed SSTs was essential in establishing the chain of cause and effect from SST anomalies to NAO. Previous studies have suggested that extra-tropical ocean surface heat fluxes may be over-estimated in atmospheric model simulations forced with prescribed SSTs[28]. Our results, however, imply that the extra-tropical (as well as tropical) evaporative heat flux, and the SSTs beneath them, may be central to the skill of our simulation of the NAO. Work is now required to resolve these differences and to understand the interannual and longer-timescale predictability of the SST pattern in Fig. 3a. This will involve using a fully coupled model[28,30] where synoptic and longer-timescale forcings of the ocean by the atmosphere are included. □

1. Kutzbach, J. E. Large-scale features of monthly mean Northern Hemisphere anomaly maps of sea-level pressure. *Mon. Weath. Rev.* **98**, 708–716 (1970).
2. Wallace, J. M. & Gutzler, D. S. Teleconnections in the geopotential height field during Northern Hemisphere winter. *Mon. Weath. Rev.* **109**, 784–812 (1981).
3. Rogers, J. C. Patterns of low-frequency monthly sea level pressure variability (1899–1986) and associated wave cyclone frequencies. *Q. J. R. Meteorol. Soc.* **122**, 1385–1414 (1996).
4. Ting, M. & Lau, N.-C. A diagnostic and modelling study of the monthly mean wintertime anomalies appearing in a 100-year GCM experiment. *J. Atmos. Sci.* **50**, 2845–2867 (1993).
5. Sutton, R. T. & Allen, M. R. Decadal predictability of North Atlantic sea surface temperature and climate. *Nature* **388**, 563–567 (1997).
6. Bjerknes, J. Atlantic air-sea interaction. *Adv. Geophys.* **10**, 1–82 (1964).
7. Daly, A. W. The response of North Atlantic sea surface temperature to atmospheric forcing processes. *Q. J. R. Meteorol. Soc.* **104**, 363–382 (1978).
8. Cayan, D. R. Latent and sensible heat flux anomalies over the northern oceans: The connection to monthly atmospheric circulation. *J. Clim.* **5**, 354–369 (1992).
9. Deser, C. & Blackmon, M. L. Surface climate variations over the North Atlantic ocean during winter: 1900–1989. *J. Clim.* **6**, 1743–1753 (1993).
10. Namias, J. Seasonal persistence and recurrence of European blocking during 1958–1960. *Tellus* **16**, 394–407 (1964).
11. Ratcliffe, R. A. S. & Murray, R. New lag associations between North Atlantic sea temperatures and European pressure, applied to long-range weather forecasting. *Q. J. R. Meteorol. Soc.* **96**, 226–246 (1970).
12. Palmer, T. N. & Sun, Z. A modelling and observational study of the relationship between sea surface temperature in the northwest Atlantic and the atmospheric general circulation. *Q. J. R. Meteorol. Soc.* **111**, 947–975 (1985).
13. Davies, J. R., Rowell, D. P. & Folland, C. K. North Atlantic and European seasonal predictability using an ensemble of multi-decadal AGCM simulations. *Int. J. Climatol.* **17**, 1263–1284 (1997).
14. Latif, M. & Barnett, T. P. Causes of decadal variability over the North Pacific and North America. *Science* **266**, 634–637 (1994).
15. Grötzner, A. M., Latif, M. & Barnett, T. P. A decadal climate cycle in the North Atlantic ocean as simulated by the ECHO coupled GCM. *J. Clim.* **11**, 831–847 (1998).
16. Frankignoul, C. & Hasselmann, K. Stochastic climate models, Part II: Application to sea-surface temperature anomalies and thermocline variability. *Tellus* **29**, 289–305 (1977).
17. Frankignoul, C. Sea surface temperature anomalies, planetary waves and air-sea feed-back in the middle latitudes. *Rev. Geophys.* **23**, 357–390 (1985).
18. Hall, C. D., Stratton, R. A. & Gallani, M. L. *Climate Simulations with the Unified Model: AMIP Runs* (Clim. Res. Tech. Note 61, UK Meteorol. Office, Bracknell, 1995).
19. Lamb, P. J. On the mixed-layer climatology of the north and tropical Atlantic. *Tellus A* **36**, 292–305 (1984).
20. Walker, G. T. & Bliss, E. W. World Weather V. *Mem. R. Meteorol. Soc.* **4**, 53–84 (1932).
21. Van Loon, H. & Rogers, J. C. The seesaw in winter temperatures between Greenland and northern Europe. Part I: General description. *Mon. Weath. Rev.* **106**, 296–310 (1978).
22. Hurrell, J. W. Influence of variations in extratropical wintertime teleconnections on Northern Hemisphere temperature. *Geophys. Res. Lett.* **23**, 665–668 (1996).
23. Hulme, M. A 1951–80 global land precipitation climatology for the evaluation of general circulation models. *Clim. Dyn.* **7**, 57–72 (1992).
24. Van den Berg, W. D. The role of various weather parameters and the use of worst-case forecasts in prediction of gas sales. *Meteorol. Applicat.* **1**, 33–37 (1994).
25. Kushnir, Y. Interdecadal variations in North Atlantic sea surface temperature and associated atmospheric conditions. *J. Clim.* **7**, 141–157 (1994).
26. Xie, S. P. A pan-Atlantic decadal climate oscillation. *Geophys. Res. Lett.* **25**, 2185–2188 (1998).
27. Blackmon, M. L. & Lau, N.-C. Regional characteristics of the Northern Hemisphere wintertime

ciruculation: A comparison of the simulation of a GFDL general circulation model with observations. *J. Atmos. Sci.* **37**, 497–514 (1980).
28. Saravanan, R. Atmospheric low-frequency variability and its relationship to midlatitude SST variability: Studies using the NCAR climate system model. *J. Clim.* **11**, 1386–1404 (1998).
29. Molinari, R. L., Mayer, D. A., Festa, J. F. & Bezdek, H. F. Multiyear variability in the near-surface temperature structure of the midlatitude western North Atlantic ocean. *J. Geophys. Res.* **102**, 3267–3278 (1997).
30. Barsugli, J. J. & Battisti, D. S. The basic effects of atmosphere–ocean thermal coupling on midlatitude variability. *J. Atmos. Sci.* **55**, 477–493 (1998).

Distortion of isochronous layers in ice revealed by ground-penetrating radar

David G. Vaughan*, **Hugh F. J. Corr***, **Christopher S. M. Doake*** & **Ed. D. Waddington**†

* *British Antarctic Survey, Madingley Road, Cambridge CB3 0ET, UK*
† *Geophysics Program, University of Washington, Box 351650, Seattle, USA*

In addition to measuring ice-sheet thickness, ground-penetrating radar can be used to delineate reflections in ice sheets[1–3]. These reflections are generally accepted to result from layers of isochronous deposition of snow and can reveal much about the dynamics of the ice flow. Here we present ground-penetrating radar data from Fletcher Promontory, Antarctica, which show arches and troughs in isochronous ice layers to a depth of 100 m. We demonstrate that the origin of these features can be determined by their growth with depth, and many features result from local anomalies in accumulation rate which can be correlated with the ice surface slope. One arch appears to be the result of a local anomaly in vertical strain-rate. Its proximity to the ice divide, width, and growth with depth, indicate that this arch is one of a class of features postulated by Raymond[4] but not previously shown to exist in the field. Such a feature is an indication of the nonlinear rheology of ice and requires that palaeoclimate records from ice cores extracted from the vicinity of ice divides underlain by similar features should be specifically corrected for such effects on ice-flow.

Fletcher Promontory, Antarctica, is a 500-m thick ice cap, atop a shear-sided, inclined mesa between Rutford Ice Stream and Carlson Inlet (Fig. 1). The mean annual air temperature is about −20 °C and ice flow is only a few metres per year (ref. 5), indicating that the ice is frozen to its bed. Snow accumulation close to the crest was measured over one year as $(320 \pm 60) \, kg \, m^{-2} \, yr^{-1}$.

Figure 2 shows a 15-km-long ground-penetrating radar (GPR) section collected over Fletcher Promontory. The section shows many internal horizons in the uppermost 100 m, which are thought to result from density variations related to depositional processes[6,7]; but as the wavelengths used are greater than the thickness of the snow layer from any one precipitation event, each internal horizon corresponds to interference from several layers[8]. Indeed, some layers were resolved into multiple horizons by using 200-MHz GPR data not presented here.

The internal horizons shown in Fig. 2b undulate to give arches and troughs which are unrelated to bed topography. Figure 3 shows the dip of predicted particle paths across Fletcher Promontory, together with the dip of lines drawn down through arches and troughs. The agreement suggests that the arches and troughs result from burial processes, not from the flow of ice over topography.

Defining the x-axis as horizontal and the z-axis as vertically downwards, the burial rate of ice from the surface ($x = 0$, $z = 0$)